IEEE Access
Multidisciplinary | Rapid Review | Open Access Journal

Received 13 November 2022, accepted 1 December 2022, date of publication 5 December 2022,
date of current version 12 December 2022.

Digital Object Identifier 10.1109/ACCESS.2022.3226812

RESEARCH ARTICLE

Solar Speckle Image Deblurring With Deep Prior Constraint Based on Regularization

YAHUI JIN[1], MURONG JIANG[1], LEI YANG[2], SIZHONG ZOU[2], LINHAO DENG[1], AND JUNYI CHEN[2]

[1]School of Information Science and Engineering, Yunnan University, Kunming, Yunnan 650500, China
[2]Yunnan Observatories, Chinese Academy of Sciences, Kunming, Yunnan 650216, China

Corresponding author: Murong Jiang (jiangmr@ynu.edu.cn)

This work was supported in part by the National Natural Science Foundation of China under Grant 11773073, in part by the Yunnan University Science and Technology Innovation Team Support Project under Grant IRTSTYN, and in part by the Yunnan University Graduate Research Innovation Fund Project under Grant 2021Y273.

ABSTRACT The solar speckle image has the characteristics with single features, more noise, and blurred local details. Most of the existing deep learning deblurring methods for solar speckle images have some problems, such as high-frequency loss, artifact generation, and dependence on the paired image. In this paper, a deep prior deblurring method fusing the regularization model and prior constraint network is proposed. Firstly, the traditional handcrafted regularization priors are added to the network parameterized blind deconvolution model. The image gradient prior and blur kernel initial parameters are respectively used to the network parameterization process of two variables in the blind deconvolution model, which are the latent clean image variables and blur kernel variables. After that, the solar speckle image deep prior deblurring model is established. Secondly, the blur kernel generation network input is estimated by using the atmospheric point spread function (PSF) to improve the model convergence speed. Thirdly, a latent clean image generation network including joint gradient branching and Feature Pyramid Network (FPN) structure is designed to enhance image local edge details. Finally, a joint loss function including pixel loss, image prior loss, and mean squared error (MSE) loss is introduced to guide the model for alternate training. It can obtain the best parameter values of latent clean image and blur kernel, and achieve the solar speckle image high-resolution reconstruction. The experimental results show that the proposed method can eliminate the dependence on the reference image, and the reconstructed image has less noise and more obvious high-frequency details, faster network convergence, and two evaluation indicators of Peak Signal Noise Ratio (PSNR) and Structural Similarity (SSIM) are significantly improved.

INDEX TERMS Solar speckle image, regularization model, deep image prior, point spread function.

I. INTRODUCTION

Due to the interference of atmospheric turbulence, the solar speckle images taken by ground-based telescopes are severely blurred and require high-resolution reconstruction by image processing. High-resolution reconstruction techniques can be divided into two categories: one is the speckle imaging method [1], [2], [3] based on the statistics with each order, and the other is the multi-frame blind deconvolution and phase difference method, which is based on instantaneous deconvolution [4]. However, these methods require more prior knowledge in the reconstruction process, such as atmospheric seeing and speckle interference function [5], and require more image frames, resulting in a large amount of calculation in the reconstruction process, which cannot meet the real-time data processing requirements of astronomical observation.

As deep learning is widely used in computer vision and image processing, using deep learning techniques to reconstruct solar speckle images, and improve the solar observation data analysis and processing capability has become one of the hot spots in solar observation image processing [6].

The associate editor coordinating the review of this manuscript and approving it for publication was Md. Moinul Hossain.

In recent years, network model represented by a generative adversarial network (GAN) [7] has achieved better performance than traditional algorithms in many image processing tasks, such as image segmentation [8], and image denoising [9]. Most deep learning-based deblurring algorithms for solar speckle images [10], [11], [12], [13], [14] also use GAN as a framework, and remove artifacts and noises in blurred image by learning the end-to-end mapping function from blurred image to reference image. However, since the blurring of solar speckle images is caused by the irregular changes of atmospheric turbulence, which makes the blurring distribution of solar speckle images taken at different moments vary greatly. And the model trained several minutes ago may not be suitable for the solar speckle image taken several minutes later and needs to be retrained. The newly taken solar speckle images do not have corresponding real images in a short period time, resulting in supervised methods cannot be applied to real-time reconstruction of solar speckle images that rely on blurred images and their corresponding reference images. To solve the problem of insufficient reference images, in 2018, Ulyanov et al. [15] constructed an unsupervised network model deep image prior (DIP), which replaced the image variables in the energy function by the output of a deep convolutional neural net (ConvNet) with noise as input. In this way, the image prior can be captured by the hyperparameter of the ConvNet, and the output image is determined by the parameter of the ConvNet [16]. The model effectively solves the problem that the reconstruction results depend on the reference image, but the deblurring performance is not well. After that, Mataev et al. [17] integrated Regularization by Denoising (RED) [18] into DIP to improve the deblurring performance of the DIP model. Shocher et al. [19] used two separated hourglass networks to capture both latent clean image and blur kernel prior, respectively. However, the hourglass network is designed to generate natural images and is limited to capture the prior of blur kernels. Ren et al. [11] replaced the blur kernel generation network with fully connected network (FCN) to make up for the limited of hourglass network in reconstructing blur kernel, which further improved the image reconstruction result. Mirza et al. [20] proposed a conditional generation adversarial network, which replaced noise with other prior information as network input to improve the network prediction results. Fumio et al. [21] and Sun et al. [22] inputed medical noise images as prior information into generate network, and obtained better image denoising results. These methods have achieved good results in image deblurring calculation, but there are some deficiencies for solar speckle image reconstruction, such as slow network convergence and blurred local edges, which are due to the large randomness of the generated results when the network with noise as input, as well as the solar speckle images usually contain single structural features, more noise, and blurred local details.

For the existing deblurring algorithms depend on the reference image, there are problems when DIP-based methods are used for solar speckle images reconstruction, such as slow network convergence and blurred local edges, a deep prior deblurring method fusing the regularization model and prior constraint network is proposed, and the method is named as Solar Speckle Image Deep Prior Deblurring (SSIDPD). Firstly, the TV regularization prior [23] and L_1 regularization prior [24] are added to the blind deconvolution model of network parameterized. And the prior information such as image gradient prior and blur kernel initial parameters are respectively used to the network parameterization process of two variables in the blind deconvolution model, which are the latent clean image variables and blur kernel variables. After that, a deep prior deblurring model is established for solar speckle image. Secondly, according to the solar speckle image blur kernel characteristics, the atmospheric point spread function (PSF) output is used to blur kernel generation network FCN input to capture the blur kernel prior. Thirdly, the noise and blur image are used to the Latent Clean Image Generation Network (LCIGN) input to capture the latent clean image prior. Finally, a joint loss function including pixel loss, image prior loss and MSE loss is introduced to guide the model for alternate training. It can obtain the best parameter values of the latent clean image and blur kernel, and achieve high-resolution reconstruction of the solar speckle image. The experimental results show that the proposed SSIDPD method can get rid of the dependence on the reference image, and the reconstruction results have more obvious edge details, less noise and artifacts, network model converges faster, and both evaluation indexes of Peak Signal Noise Ratio (PSNR) and Structural Similarity (SSIM) are significantly improved.

SSIDPD has three contributions for solar speckle images reconstruction:

(1) The handcrafted regularization prior, image gradient prior, and blur kernel initial parameters are merged into the blind deconvolution model of network parameterized, which can train the reconstruction network without solar speckle reference image.

(2) The atmospheric PSF is used to give approximate estimate of the blur kernel generation network input, which accelerates the network model convergence.

(3) A latent clean image generative network LCIGN is designed to reconstruct the solar speckle image, which can capture image edge details prior more effectively.

The contents of this paper are arranged as follows: In the second part, the proposed SSIDPD method is introduced in detail, including the establishment of a deep prior deblurring model for solar speckle image, blur kernel generation network with atmospheric PSF output as input, and the design of the generation network LCIGN; In the third part, some experiments and result analysis are preformed to verify SSIDPD effectiveness; In the fourth part, the advantages and disadvantages of SSIDPD are summarized.

II. METHODOLOGY

The proposed SSIDPD method includes three parts: (1) constructing the solar speckle image deep prior deblurring model.

(2) estimating the input of the blur kernel generation network by using the atmospheric PSF. (3) designing the reconstruction network LCIGN.

A. SOLAR SPECKLE IMAGE DEEP PRIOR DEBLURRING MODEL

When the blur kernel remains spatially invariant, image recovery can be viewed as a linear blind deconvolution problem, and the blur image $y \in \mathbb{R}^{d\times m\times n}$ may be expressed as:

$$y = k * x + n \tag{1}$$

where $*$ is a two-dimensional convolution operation, $k \in \mathbb{R}^{h\times w}$ is an unknown blur kernel, $x \in \mathbb{R}^{d\times m\times n}$ is a latent clean image,$n \in \mathbb{R}^{d\times m\times n}$ is an additive Gaussian white noise with noise level σ, and d denotes the number of image channels. Our aim to recover the latent clean image x from the blurred image y.

In this proposed deblurring framework, the latent clean image x and the blur kernel k are parameterized as the output of ConvNet like

$$x = f_\theta(z_x), \quad k = g_\rho(z_k) \tag{2}$$

The process is shown as follows

$$f : \{z_x \in \Omega_1 \mid p(z_x) \neq 0\} \times \Theta_1 \xrightarrow{\text{ConvNet}} I_1, \quad (z_x, \theta) \to x \tag{3}$$

$$g : \{z_k \in \Omega_2 \mid p(z_k) \neq 0\} \times \Theta_2 \xrightarrow{\text{ConvNet}} I_2, \quad (z_k, \rho) \to k \tag{4}$$

where p denotes the probability density function, f and g denote different ConvNet structures, θ and ρ are the network weights of f and g, respectively, z_x and z_k are input as prior information in $f_\theta(\cdot)$ and $g_\rho(\cdot)$, respectively, Ω_1, Ω_2 are the sample spaces of z_x, z_k, respectively [25], Θ_1, Θ_2 are the weight space determined by the ConvNet structure, and I_1,I_2 are the solution spaces of x and k under the constraints of the ConvNet structure. Thus, with the solution space I_1, f maps the network with noise $z_x \in \mathbb{R}^{C'\times H'\times W'}$ and network weights θ as input to the output $x \in \mathbb{R}^{3\times \mathrm{H}\times \mathrm{W}}$ of the network model, and with the solution space I_2, g maps the network with initial parameters $z_k \in \mathbb{R}^{C'\times H'\times W'}$ and network weights ρ as input to the output $k \in \mathbb{R}^{3\times \mathrm{H}\times \mathrm{W}}$ of the network model.

Substituting $x = f_\theta(z_x)$ and $k = g_\rho(z_k)$ into the linear blind deconvolution model (1), the model can be rewritten as

$$y = g_\rho(z_k) * f_\theta(z_x) + n \tag{5}$$

The latent clean images x and the blur kernel k will be obtained as

$$\begin{aligned}(\theta^*, \rho^*) &= \underset{(\theta,\rho)}{\operatorname{argmin}} \left\| f_\theta(z_x) * g_\rho(z_k) - y \right\|_2^2 \\ x &= f_{\theta^*}(z_x), k = g_{\rho^*}(z_k)\end{aligned} \tag{6}$$

In order to remove the noise and artifacts from the reconstruction results, the TV regularization prior of x and the L_1 regularization prior of k are added to (6).Then, the model can be extended as

$$\begin{aligned}&(\theta^*, \rho^*) \\ &= \underset{(\theta,\rho)}{\operatorname{argmin}} \left\| f_\theta(z_x) * g_\rho(z_k) - y \right\|_2^2 + \delta TV(x) + \eta \|k\|_1\end{aligned} \tag{7}$$

where $x = f_{\theta^*}(z_x), k = g_{\rho^*}(z_k)$, δ and η denote the two regularization parameters. Although model (7) can remove the noise and artifacts in the reconstruction results, there also exist some deficiencies of local edge blurring in the reconstruction results. Considering that there are still a large amount of reusable gradient information in the blur image y, using the generative network $f_\theta(\cdot)$ to capture the prior of x from y and z_x at the same time, we modify x in (2) with

$$x = f_\theta(z_x, y) \tag{8}$$

The parameterization process for the modified x is shown as

$$\begin{aligned}f : \left\{z_x \in \Omega_1, y \in \mathbb{R}^{d\times m\times n} \mid p(z_x) \neq 0\right\} \times \Theta_1 &\xrightarrow{\text{ConvNet}} I_1, \\ ((z_x, y), \theta) &\to x\end{aligned} \tag{9}$$

According to (8), we modify (7) again to obtain the solar speckle image deep prior deblurring model as follows

$$\begin{aligned}(\theta^*, \rho^*) = \underset{(\theta,\rho)}{\operatorname{argmin}} &\left\| f_\theta(z_x, y) * g_\rho(z_k) - y \right\|_2^2 \\ &+\delta \|f_\theta(z_x, y)\|_{TV} + \eta \left\| g_\rho(z_k) \right\|_1\end{aligned} \tag{10}$$

Model (10) can be solved by analogy with the alternating minimization algorithm like the traditional blind deconvolution model [26], [27], [28]. The parameters in two networks f_θ and g_ρ will also be optimized in an alternating manner. In this paper, model (10) is decomposed into two subproblem as shown in equation (11)-(12)with

$$\theta^* = \underset{\theta}{\operatorname{argmin}} \left\| f_\theta(z_x, y) * g_\rho(z_k) - y \right\|_2^2 + \delta \|f_\theta(z_x, y)\|_{TV} \tag{11}$$

$$\rho^* = \underset{\rho}{\operatorname{argmin}} \left\| f_\theta(z_x, y) * g_\rho(z_k) - y \right\|_2^2 + +\eta \left\| g_\rho(z_k) \right\|_1 \tag{12}$$

The specific alternative solution process is shown in Algorithm 1. When using the ADAM [29] optimizer to update the network parameters of f_θ, the parameters of g_ρ are fixed, and vice versa.

B. ESTIMATE THE INPUT FOR BLUR KERNEL GENERATION NETWORK

It can be seen from model (10) that z_k will be used as a prior input to the blur kernel generation network $g_\rho(\cdot)$. The blur kernel $g_\rho(z_k)$ also be regarded as a mapping function for the network $g_\rho(\cdot)$ to learn a latent vector z_k to $g_\rho(z_k)$. We consider the $g_\rho(\cdot)$ with the atmospheric PSF output as input to accelerate the convergence of the blur kernel generation network, the reason is that the atmospheric PSF

Algorithm 1 Alternating Minimization Algorithm for Solving Model (7)

Input: blur image y, maximum number of iterations T, Gaussian noise z_x, blur kernel initial parameters z_k.
Output: blur kernel k and latent clean image x.
1: $k = g_\rho^0(z_k)$
2: for t = 1 to T do
3: $x = f_\theta^{t-1}(z_x, y)$
4: Compute the gradient w.r.t. g_ρ by
$$\underset{\rho}{\operatorname{argmin}} \left\| f_\theta^{t-1}(z_x, y) * g_\rho^{t-1}(z_k) - y \right\|_2^2 + \eta \left\| g_\rho^{t-1}(z_k) \right\|_1$$
5: Update g_ρ^t using the ADAM algorithm
6: $k = g_\rho^t(z_k)$
7. Compute the gradient w.r.t. f_θ by
$$\underset{\theta}{\operatorname{argmin}} \left\| f_\theta^{t-1}(z_x, y) * g_\rho^t(z_k) - y \right\|_2^2 + \delta \left\| f_\theta^{t-1}(z_x, y) \right\|_{TV}$$
8: Update f_θ^t using the ADAM algorithm
9: end for
10: x $= f_\theta^T(z_x, y)$, k $= g_\rho^T(z_k)$

can reflect many blur kernel properties of the solar speckle image [12].

From the theory of atmospheric dynamics [30], the general form of the atmospheric PSF is usually given by Hankel transform of the modulation transfer function, and the form is as follows

$$P(r_0) = \int_0^\infty J_0\left(\frac{\lambda v^2}{2\pi}\right) \exp\{-0.5\, D_s(v)\}\, v dv \tag{13}$$

where $\exp\{-0.5\, D_s(v)\}$ is the modulation transfer function, $J_0\left(\frac{\lambda v^2}{2\pi}\right)$ is the order zero Bessel function, v is the spatial frequency, and λ denotes the atmospheric wavelength. $D_s(v)$ is the phase space structure function, which represents the mean squared difference of the phase between any two points in the focal plane of the telescope, as shown in following.

$$D_S(v) = 6.88\left(\frac{\lambda v}{2\pi r_0}\right)^{5/3} \tag{14}$$

where r_0 is the atmospheric seeing, which is an important physical parameter to measure the intensity of atmospheric turbulence disturbance. It can be seen from (13) that given different values of r_0, different z_k can be obtained $z_k = \mathrm{P}(r_0)$.

Since z_k estimated by (13) is a one-dimensional vector, if $g_\rho(\cdot)$ is a linear fully connected network, then we can directly input z_k into $g_\rho(\cdot)$ as a prior, and then decide the output size of the blur kernel $g_\rho(z_k)$ in the last fully connected layer. However, if $g_\rho(\cdot)$ is a deep convolutional network, usually need the space size of z_k and $g_\rho(z_k)$ are the same during the mapping process, then we need to determine the size of z_k in advance. Since the fully connected network is used as the blur kernel generation network in this paper, thus the number of nodes in the last fully connected layer is determined by the size of the blur kernel.

From the principle of optical imaging, the degradation of image quality can be considered as an image taken using an aperture of r_0. When r_0 is given, the size of the blur kernel n_{pix} can be calculated by (15) [31] likes

$$n_{pix} = \frac{\alpha}{\alpha_{pix}} \tag{15}$$

where α is the angular second, defined as $\alpha = 2.021 \times 10^5 \times \frac{\lambda}{r_0}$, and α_{pix} denotes the size of a single pixel corresponding to the angular second.

C. DESIGN THE RECONSTRUCTED NETWORK

Compared to natural images, the texture structure of the solar speckle images is more complex, and the contextual information is mainly reflected in the scattered shapes of rice grains and the gaps between rice grains [13]. Therefore, it is necessary to design a special network structures f to express the priors of latent clean image. Due to the sparseness of the blur kernel, a simple FCN is used to capture the prior of blur kernel from the latent vector z_k. In natural image processing, the FPN [32] has achieved good results, but it has the disadvantage of local edge blurring for the solar speckle image with single features, low contrast, and more noise. In this paper, we construct the LCIGN module to make up for the deficiency of local edge blurring of the existing network reconstruction results. The reconstruction network consists of two generator network modules, the latent clean image generation network module LCIGN, the blur kernel generation network module FCN, and the reconstructed network structure is shown in Figure 1.

In order to enhance the edge details of the image, the LCIGN network is designed with a joint reconstruction of FPN network structure and gradient branches, because the FPN network can capture smaller details, and at the same time, incorporating a large amount of reusable gradient information in the blur image y into the reconstruction result of the FPN network can effectively enhance the edge details of the image. And also in order to ensure that the added individual branch Gradient Enhanced Network 2 (GEN2) can obtain a valid and true gradient image from y, a loss function needs to be introduced to constrain the mapping space of GEN2. To achieve this purpose, we first add the gradient enhanced network branch 1 (GEN1) to the FPN network and then obtains the gradient information in the reconstruction result of the FPN network, and the result is recorded as the target gradient image, and then calculates the mean absolute error (MAE) of the target gradient image and the gradient image obtained by GEN2, and finally adds the error result to the total loss function for parameter search.

1) CONSTRUCT THE LCIGN NETWORK MODULE

Inspired by Ma et al. [33] and Kupyn et al. [34], the LCIGN network module is constructed by using the FPN network structure and gradient branching joint reconstruction, and the structure of the LCIGN network module is shown in Figure 2 as follow. Among them, Ma et al. [33] use the gradient image of the clean image as a reference, and guide the gradient branch to recover the high-resolution gradient image from

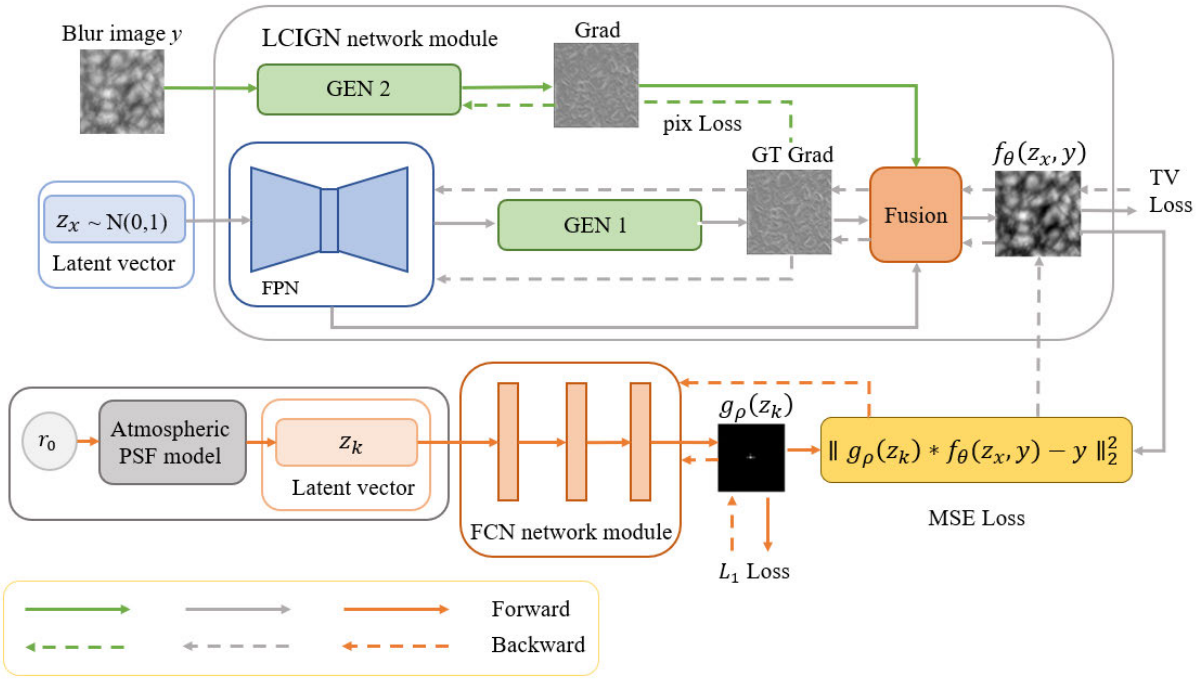

FIGURE 1. Reconstruction network structure.

the low-resolution gradient image of the blurred image, and provide a spatial structure prior for the image reconstruction process to recover the local details in the image.

Unlike the above work, the solar speckle image deblurring model established in this paper does not involve a clean reference image. To recover the local details of the solar speckle image as a spatial structure prior, we add the gradient branch GEN1 after the FPN network to obtain the gradient information of the reconstructed results. This design is based on the fact that the FPN reconstructed solar speckle image has less noise in the neural blind restoration model, and the powerful prior expression ability of the GEN1 structure can directly obtain the gradient image with higher resolution from the FPN network reconstruction result, so that the gradient image can be used as the target gradient image to guide the gradient branch GEN2 to recover the gradient image with higher resolution from the gradient image containing a lot of noise. The experimental results show that the design can effectively obtain the gradient information of the blured image and recover the local edge details. In addition, the Residual-in-Residual Dense Block (RRDB) residual module [35] used in the gradient branch can not only further deepen the gradient information, but also improve the training process stability.

2) BLUR KERNEL GENERATION NETWORK

Due to the sparsity of the blur kernel of the solar speckle image, similar as Ren et al. [11]. In this paper, a simple FCN is used as the generative network structure of the blur kernel g. It consists three layers with the input layer, the hidden layer, and the output layer. The number of nodes in the input layer is 500, the number of nodes in the output layer is ${n_{pix}}^2$, and the number of nodes in the hidden layer is 1000. n_{pix} is the size of the blur kernel, and the calculation process is shown in (15). To ensure that the blur kernel always satisfies the non-negative and equation constraint, the SoftMax nonlinear layer is applied to the output layer. The network also needs to be rescaled to a 2D $n_{pix} \times n_{pix}$ size blur kernel after output. The structure of the blur kernel generation network g is shown in Figure 3 as follow.

3) JOINT LOSS FUNCTION

In order to ensure the fidelity of image reconstruction, we use MSE loss to optimize the neural blind restoration model of solar speckle images. In addition to the MSE loss L_{MSE}, TV regularization loss L_{TV} and L_1 regularization loss L_{reg} are added to constrain the mapping space of f and g, respectively. To ensure that the gradient branch GEN2 can restore high-resolution gradient image, the pixel loss L_{pix} is used to force GEN2 to perform parameter search.

The total loss function is shown in (16).

$$L_{\text{total}} = L_{\text{MSE}} + \varrho L_{\text{pix}} + \delta L_{\text{TV}} + \eta L_{\text{reg}} \tag{16}$$

where

$$L_{\text{reg}}(k) = \sum_{i=1}^{w_k} \sum_{j=1}^{h_k} \left(\left|k_{i,j}\right|\right) \tag{17}$$

$$L_{\text{pix}}(z_x, y) = \frac{1}{w_l H_l} \sum_{m=1}^{w_l} \sum_{n=1}^{H_l} \| G_{\text{EGN2}}(y)_{m,n} - G_{\text{EGN1}}(F(z_x, y))_{m,n} \|_1 \tag{18}$$

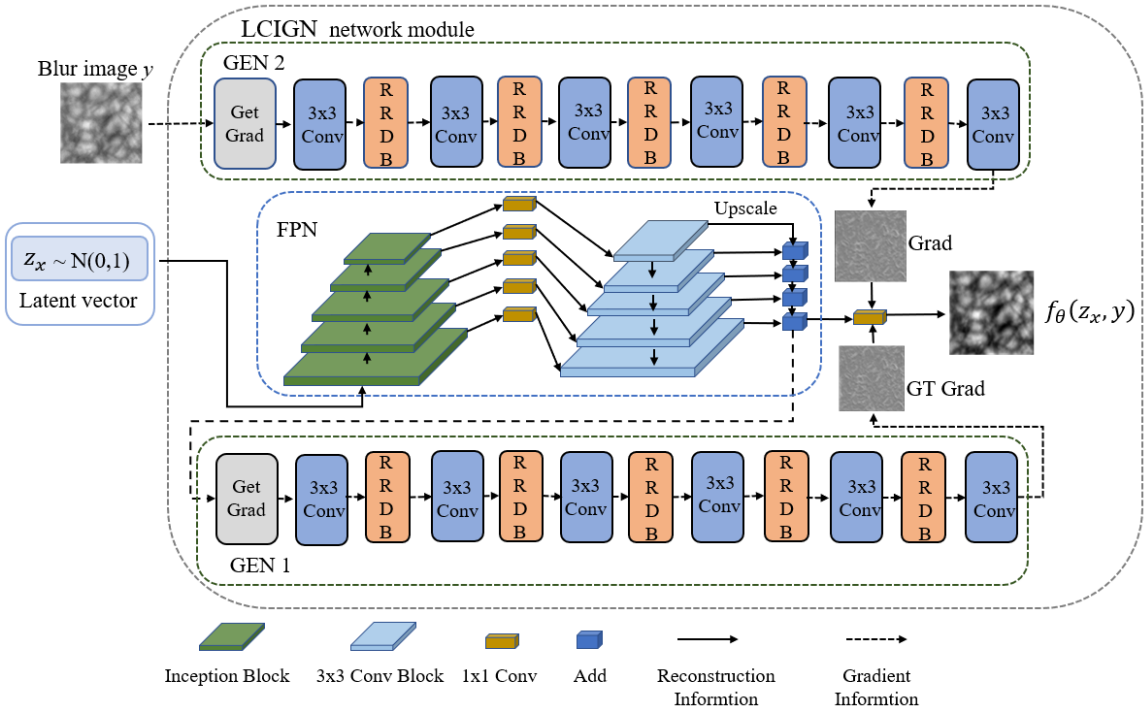

FIGURE 2. LCIGN network module structure.

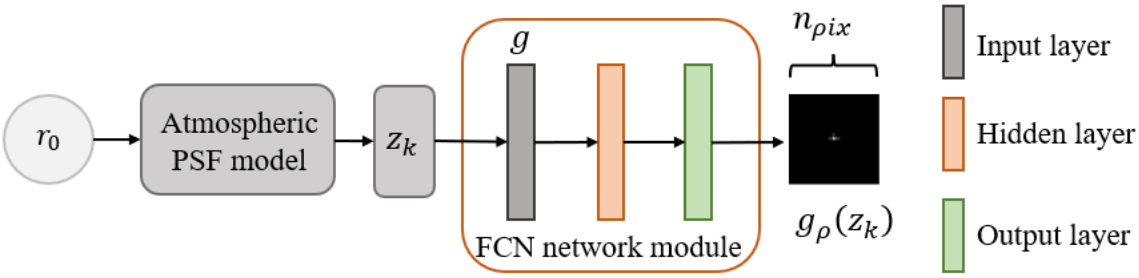

FIGURE 3. Blur kernel generation network structure.

$$L_{\mathrm{MSE}}(z_x, z_k, y) = \left\| G_{\mathrm{image}}(z_x, y) * G_{\mathrm{kernel}}(z_k) - y \right\|_2^2 \quad (19)$$

$$L_{\mathrm{TV}}(x) = \sum_{i=1}^{w_x} \sum_{j=1}^{h_x} \sqrt{\left(x_{i+1,j} - x_{i,j}\right)^2 + \left(x_{i,j+1} - x_{i,j}\right)^2} \quad (20)$$

where G_{image} denotes the latent clean image reconstruction network, G_{kernel} denotes the blur kernel reconstruction network, w_l and H_l are the feature image dimensions, w_x and h_x denote the height and width of the latent clean image, w_k and h_k denote the height and width of the blur kernel, G_{EGN2} denotes the gradient reconstruction branch EGN2, G_{EGN1} denotes the obtain gradient branch EGN1, and F is the FPN network. δ and η denote the regularization parameters in the loss function, and ϱ denotes the coefficient of pixel loss. In order to make the balance between the loss function items, this paper sets δ, η, and ϱ as 0.045, 0.008, and 0.001, respectively, through repeated experiments.

III. EXPERIMENTAL RESULTS

A. DATA SETS

In our experiments, we use the highly blurred solar speckle images taken by the Fuxian Lake Solar Telescope of Yunnan Observatory as the dataset, because the unsupervised model we construct only needs to input the blurred images into the network for iteration to achieve blind deblurring of the images. Since captured solar speckle blurred images are 2560×2160 in size, directly inputting the blurred images into the network model for iteration will lead to an explosion of computation of the network parameters, and thus the dataset needs to be cropped. Each solar speckle image of size 2560×2160 is divided into four sub-blocks, each with a pixel size of

TABLE 1. Comparison with other methods.

Medthod	PSNR	SSIM	MSE
Zhu *et al*. [24]	18.2469	0.5424	975.1
Shocher *et al*. [19]	15.4092	0.3464	1817.4
Wang *et al*. [16]	18.3866	0.5383	942.9
Ren *et al*. [11]	19.0254	0.6534	813.8
SSIDPD	**19.3491**	**0.6741**	**775.3**

1024×1024, and then the segmented sub-blocks are used for the network model training.

B. TRAINING PROCESS

To accelerate the convergence speed of the model and avoid the nonconvex optimization problem, we first divide (16) into two subproblems and then update the network parameters of f_θ and g_ρ alternately using optimizer Adam. While updating the parameters of the f_θ network, the parameters of the g_ρ network are frozen and vice versa.Typically, we set the number of iterations per image to 5000, and then set the initial learning rates of f_θ and g_η to 1×10^{-4} and 0.01, respectively, and multiply them by 0.5 for decay when the number of iterations reaches 2000, 3000, and 4000. All experiments in this paper were performed on a single Nvidia 1080ti GPU. Although GEN1 and GEN2 use the same network structure, the network iteration process does not need to update the parameters of GEN1, because the powerful prior expression ability of GEN1 network can also extract better gradient information without training.

C. COMPARISON WITH SIMILAR METHODS

1) QUANTITATIVE COMPARISON

In order to verify the validity of this method more accurately, the proposed method was compared with similar blind deblurring methods on PSNR, SSIM and MSE metrics, and the quantitative comparison results are shown in Table 1. From Table 1, it can be seen that the proposed method achieves better results in PSNR, SSIM and MSE indexes.

2) QUALITATIVE COMPARISON

In order to see the deblurring performance of SSIDPD more intuitively, we compare the reconstruction results of SSIDPD with other similar blind deblurring methods, including Zhu et al. [24], Shocher et al. [19], Wang et al. [16], and Ren et al. [11], and the comparison results are shown in Fig. 4. Among them, Zhu et al. [24] is the traditional multi-frame blind deconvolution algorithm (MIBD), Shocher et al. [19], Wang et al. [16], and Ren et al. [11] are the DIP-based methods. Among these methods, for the blur kernel generation network input, DIP-based methods all used noise as input, while SSIDPD used the atmospheric PSF output as input. For the latent clean image generation network input, both the DIP-based method and SSIDPD used Gaussian noise as input. Since both the MIBD algorithm and the SSIDPD method all have latent clean image regularization terms and blur kernel regularization terms, we set their regularization parameters δ and η to 0.048, 0.008, respectively.

As can be seen in Fig. 4, the blur kernel estimated by our SSIDPD contains less noise, and the estimated clean image is with more obvious local edge details, less noise, and artifacts, and the image recovery quality is visually better compared to other methods. Although Zhu et al. [24] can improve the signal-to-noise ratio by using more frames, the deconvolution process will amplify the image noise, which causes image phase inaccuracy and results in a large number of artifacts. Shocher et al. [19] used an hourglass network [15] to generate the blur kernel, but the generated blur kernel was too divergent and there were still a lot of artifacts in the reconstruction results. Wang et al. [16] added a Softmax layer after the output layer of the hourglass network to ensure blur kernel non-negative and equality constraints, and although they were able to restore the rice grain profile feature of the solar speckle image, white patches appeared on the rice grain gaps. Ren et al. [11] used FCN network to avoid the limitation of hourglass network generating blur kernel, and the white patches in the reconstructed results were reduced, but there were still noise, artifacts, and local blurred edge.

D. BLUR KERNEL GENERATION NETWORK WITH DIFFERENT INPUTS

To verify that the blur kernel generation network with atmospheric PSF output as input, which can accelerate the convergence of the network model. In this experiment, we first compare the convergence of the blur kernel loss function when blur kernel generation network with Gaussian noise, uniform noise, and the atmospheric PSF output as input, respectively. Figure 6 shows the optimization curves of blur kernel loss with respect to iterations when the blur kernel generation network with different prior as input. As shown in Figure 6, when the blur kernel generation network with atmospheric PSF output as input, the convergence of the network model is faster compared to Gaussian noise and uniform noise as input. This also confirms our idea that the network with atmospheric PSF output as input, which can be regarded as a conditional constraint to guide the network to generate blur kernel. It not only accord with the blur kernel characteristics of the solar speckle images, but also can converge with fewer iterations. This is similar to related work in conditional GAN [37], [38] that when the input is not random noise, but the associated prior information, the prediction results can be improved. In contrast, the generated results of network with noise as input are uncontrollable [20] and require a higher number of iterations to converge.

To be able to see more intuitively, the different prior are used to blur kernel generation network input, which can influence the network model convergence. Figure 5 shows a visual comparison of the intermediate evaluation results of the blur kernel generation network with different priors as input under 500, 1000, and 1500 iterations. It can be seen from Figure 5 that the blur kernel gradually becomes clearer with increasing number of iterations and eventually becomes

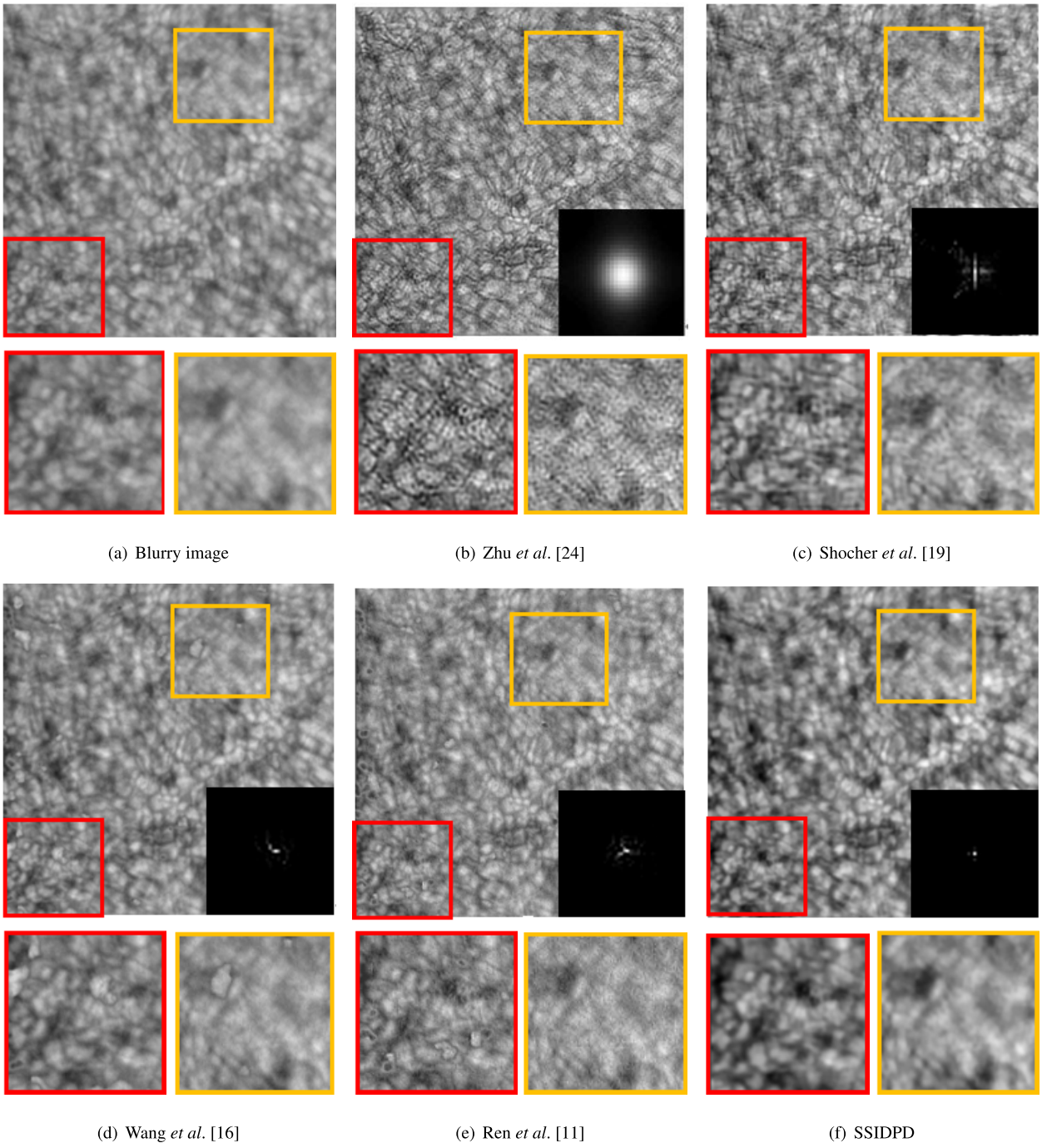

(a) Blurry image (b) Zhu *et al*. [24] (c) Shocher *et al*. [19]

(d) Wang *et al*. [16] (e) Ren *et al*. [11] (f) SSIDPD

FIGURE 4. Comparison of reconstruction results of different methods.

a point source shape. However, when the number of iterations at 500 it can be seen that the blur kernel is significantly noisier when the kernel generation network with uniform noise and Gaussian noise as input, while the blur kernel is relatively clearer when the kernel generation network with the atmospheric PSF output as input. This is consistent with our expectation that only a few iterations are needed for the network to generate clear blur kernels, reducing the latent clean image generation network solution space. This idea is further confirmed in the solar speckle image reconstruction results in Figure 7.

Figure 7 shows the comparison of reconstruction results of the solar speckle image when the blur kernel generation network respectively with uniform noise and atmospheric PSF out as input for the same number of iterations. It can also be intuitively seen from Figure 7 that the local reconstruction results of the images are better when the network with the atmospheric PSF output as input, because atmospheric

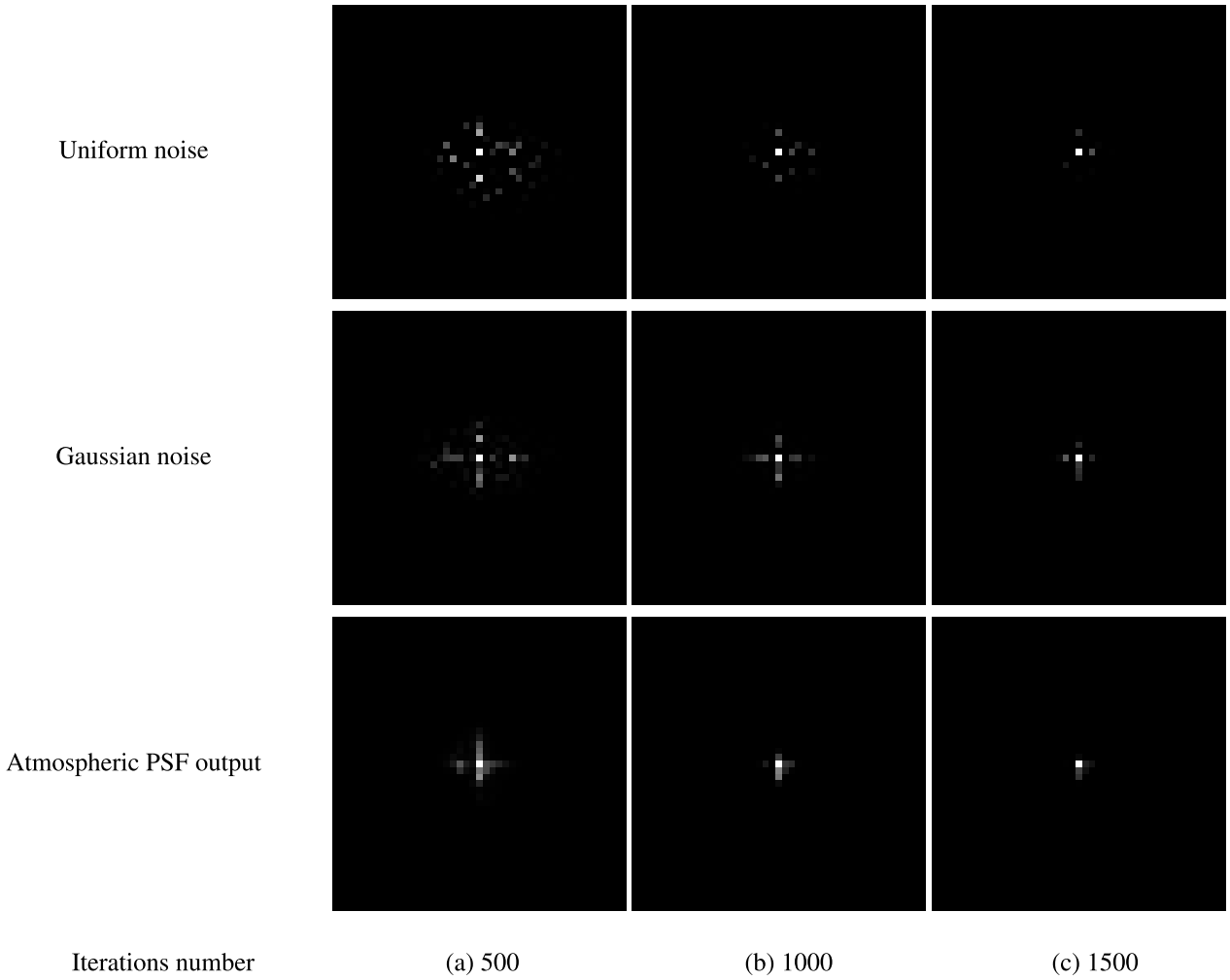

FIGURE 5. Comparison of blur kernel reconstruction results with different iterations.

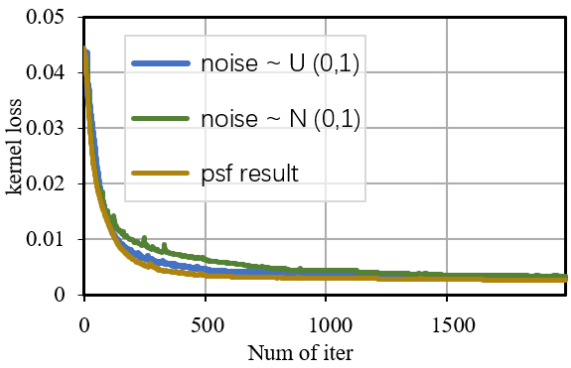

FIGURE 6. Optimization curves for blur kernel generation networks with different inputs.

PSF output is closer to the real blur kernel distribution and can be regarded as a kind of conditional prior to guide the network to generate blur kernel, which shortens the distance of generating network to capture the blur kernel prior, and can quickly reverse solution the latent clean image. However, the kernel generation network with uniform noise as input, construction results of the latent clean image show significant local defects, which may be due to the slow convergence of the blur kernel, resulting in a limited solution of latent clean images during blind deconvolution.

The quantitative evaluation in Table 2 shows that when the kernel generation network with atmospheric PSF output as input, the quality of the image reconstruction results is significantly better than the kernel generation network with uniform noise and Gaussian noise as input. This further demonstrates the effectiveness of using the atmospheric PSF output as the blur kernel generation network input to speed up the convergence of the network model, and thus blur kernel generation network with the atmospheric PSF model output as input is a good choice.

E. ABLATION EXPERIMENTS

1) GRADIENT BRANCHING VS. NO GRADIENT BRANCHING

In order to verify the effectiveness of adding the gradient branch GEN2, we evaluated the effects of removing GEN2

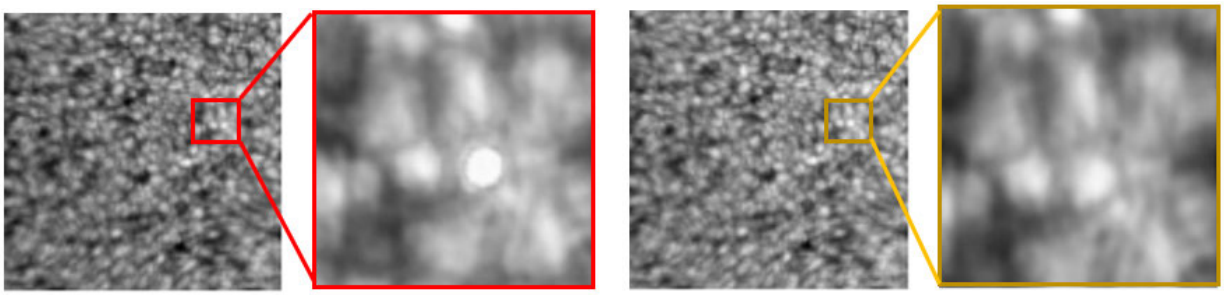

(a) Uniform noise (b) Atmospheric PSF output

FIGURE 7. Comparison of latent clean image reconstruction results with different inputs to blur kernel generation network.

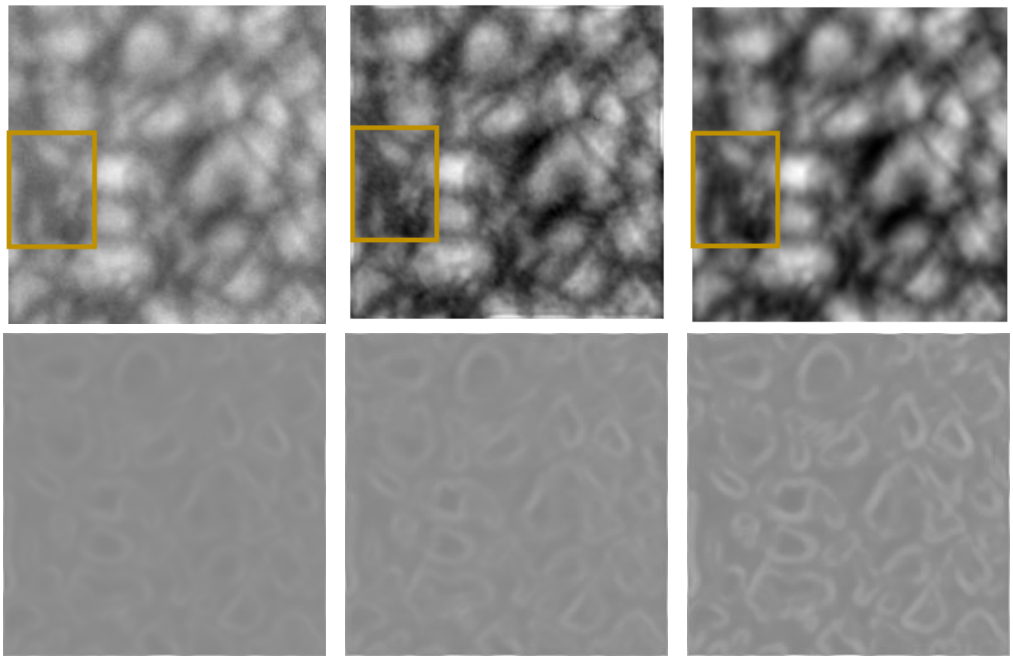

(a) Blurry image (b) LCIGN- (c) LCIGN

FIGURE 8. Comparison of the effect of gradient branch on reconstruction results.

TABLE 2. Effects of blur kernel generation network with different inputs.

Noise type	PSNR	SSIM
Uniform noise	18.2763	0.5876
Gaussian noise	19.3512	0.6131
Atmospheric PSF output	**19.5645**	**0.6456**

(LCIGN-) and adding GEN2 (LCIGN) to the reconstruction results. The quantitative evaluation in Table 3 shows that LCIGN outperforms LCIGN-, which illustrates the superiority of LCIGN with the addition of the gradient branch. From the visualization results in Figure 8, we can see that the local edges of the LCIGN- network reconstruction results are more blurred, and from the gradient image of the reconstruction results, we can also see that the gradient of LCIGN- is not obvious enough, while LCIGN can further deepen the gradient. Therefore, LCIGN can effectively enhance the blurred local edges. It also confirms the idea of our network model design, which uses a gradient branch to capture a large amount of reusable gradient information in the blurred image alone, and then incorporates it into the reconstruction result to achieve enhanced edge details. However, for the unsupervised network model, since there is no clean gradient image as the reference image, it is difficult for the gradient branch to capture the effective gradient information from the blurred image, and we can only consider obtaining the sub-optimal gradient image from the not completely recovered blur image to guide the gradient branch to reconstruct the effective gradient image from the blurred image, which is similar to the ''zero-shot'' self-supervised learning [38], which mines prior information from the inside of the blurred image to be beneficial for reconstruction.

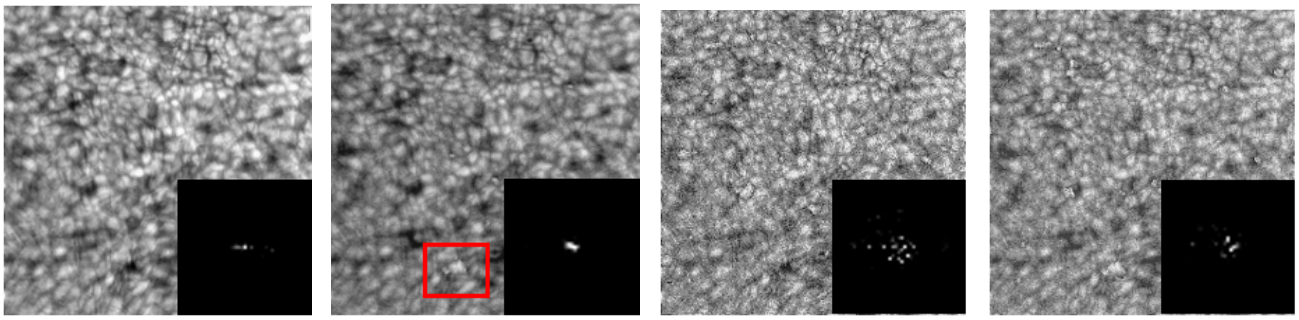

(a) SSIDPD (b) SSIDPD$_{k-}$ (c) SSIDPD$_{x-}$ (d) SSIDPD$_{x-,k-}$

FIGURE 9. Visual comparison of SSIDPD variants with different regularized priors.

TABLE 3. Effect of gradient branch.

Method	PSNR	SSIM
LCIGN-	17.6795	0.5783
LCIGN	**19.3259**	**0.6254**

TABLE 4. Quantitative comparison of SSIDPD variants with different regularization priors.

	SSIDPD	SSIDPD$_{k-}$	SSIDPD$_{x-}$	SSIDPD$_{x-,k-}$
PSNR	**19.3259**	18.6795	15.2572	16.3651
SSIM	**0.6732**	0.6135	0.5345	0.4829

2) REGULARIZED PRIOR VS. NO REGULARIZED PRIOR

We compare the results by considering four regularization priors: (i) SSIDPD, (ii) SSIDPD$_{k-}$ (with L_1 regularization prior removed), (iii) SSIDPD$_{x-}$ (with TV regularization prior removed), and (iv) SSIDPD$_{x-,k-}$ (with both regularization priors removed). As can be seen in Table 4 and Figure 9, after the regularization prior SSIDPD$_{k-}$ is removed, there is no limit to blurring kernel solution space, resulting in artifacts and white patches in the reconstruction results (as shown in the red box in (b)), but the noise of the latent clean image is suppressed. Conversely, when the TV regularization constraint SSIDPD$_{x-}$ is removed from the latent clean image, a large amount of speckle noise appears in the image. When SSIDPD does not have any regularization prior as a constraint SSIDPD$_{x-,k-}$, SSIDPD essentially degenerates into a method similar to SelfDeblur [11], and the performance of SSIDPD in capturing the deep prior of solar speckle images is severely limited with a large amount of speckle noise and artifacts. The experimental results show that the two regularization priors are good choices to suppress speckle noise and artifacts in the process of neural blind deblurring of speckle images.

IV. CONCLUSION

In this paper, we propose a deep prior deblurring method SSIDPD, which is fusing the regularization model and prior constraint network to solve the problems of existing deblurring algorithms for solar speckle images reconstruction. The proposed method gets rid of relying on solar speckle reference images, and the atmospheric PSF output is used to blur kernel generative network input to accelerate the network model convergence. Furthermore, the method merges the designed LCIGN network into the deep prior deblurring model of solar speckle image, and the network is trained by optimizing the model to capture image edge details prior more better. The experimental results show that the proposed method outperforms the existing deblurring methods in visual as well as quantitative improvements, and the two evaluation indexes of PSNR and SSIM are significantly improved.

Although the proposed method can better achieve neural blind deblurring of solar speckle images, the regularization parameters need to be selected handcrafted during the reconstruction process. In the future, we will try to introduce a loss function to optimize both the regularization parameters and the network model.

REFERENCES

[1] A. Labeyrie, "Attainment of diffraction limited resolution in large telescopes by Fourier analysing speckle patterns in star images," *Astron. Astrophys.*, vol. 53, no. 6, pp. 85–87, 1970.

[2] K. T. Knox and B. J. Thompson, "Recovery of images from atmospherically degraded short-exposure photographs," *Astrophysical J.*, vol. 127, no. 10, pp. 45–48, 1974.

[3] G. P. Weigelt, "Modified astronomical speckle interferometry 'speckle masking,'" *Opt. Commun.*, vol. 53, no. 1, pp. 55–59, 1977.

[4] Y. Y. Xiang, Z. Liu, and Z. Y. Jin, "High resolution solar image reconstruction method," *Prog. Astron.*, vol. 39, no. 1, pp. 94–110, 2016.

[5] Z. Huo and J. Zhou, "Method of astronomical image reconstruction from speckle pattern," *Prog. Astron.*, vol. 39, no. 1, pp. 74–94, 2010.

[6] W. H. Cui, M. R. Jiang, and L. Yang, "Combining MCycleGAN and RFCNN to achieve high resolution reconstruction of solar speckle image," *Comput. Sci.*, vol. 48, no. 6, pp. 38–42, 2021.

[7] I. J. Goodfellow, J. Pougetabadie, and M. Mirza, "Generative adversarial networks," in *Proc. Int. Conf. Neural Inf. Process. Syst.*, Jun. 2014, pp. 2672–2680.

[8] D. Kim and B.-W. Hong, "Unsupervised segmentation incorporating shape prior via generative adversarial networks," in *Proc. IEEE/CVF Int. Conf. Comput. Vis. (ICCV)*, Oct. 2021, pp. 7304–7314.

[9] J. Chen and H. Chao, "Image blind denoising with generative adversarial network based noise modeling," in *Proc. IEEE Conf. Comput. Vis. Pattern Recognit. (CVPR)*, Jun. 2018, pp. 3155–3164.

[10] P. Jia, Y. Huang, and B. Cai, "Solar image restoration with the CycleGAN based on multi-fractal properties of texture features," *Astrophysical J. Lett.*, vol. 127, no. 8, pp. 881–888, 2019.

[11] D. Ren, K. Zhang, Q. Wang, Q. Hu, and W. Zuo, "Neural blind deconvolution using deep priors," in *Proc. IEEE/CVF Conf. Comput. Vis. Pattern Recognit. (CVPR)*, Jun. 2020, pp. 3341–3350.
[12] P. Jia, X. Wu, and Y. Huang, "PSF–NET: A non-parametric point spread function model for ground based optical telescopes," *Astrophysical J. Lett.*, vol. 127, no. 3, pp. 654–668, 2020.
[13] F. H. Li, M. R. Jiang, and L. Yang, "A gradient-guided solar speckle image deblurring method based on generative adversarial networks," *Comput. Appl.*, vol. 41, no. 11, p. 3345, 2021.
[14] C. J. Baso, J. Cruz, and S. Danilovic1, "Solar image denoising with convolutional neural networks," *Astron. Astrophys.*, vol. 53, no. 6, pp. 89–102, 2019.
[15] V. Lempitsky, A. Vedaldi, and D. Ulyanov, "Deep image prior," in *Proc. IEEE/CVF Conf. Comput. Vis. Pattern Recognit.*, Jun. 2018, pp. 9446–9454.
[16] Z. Wang, Z. Wang, Q. Li, and H. Bilen, "Image deconvolution with deep image and kernel priors," in *Proc. IEEE/CVF Int. Conf. Comput. Vis. Workshop (ICCVW)*, Oct. 2019, pp. 9446–9454.
[17] G. Mataev, P. Milanfar, and E. Michael, "DeepRED: Deep image prior powered by RED," in *Proc. IEEE/CVF Int. Conf. Comput. Vis. (ICCV)*, Oct. 2019, pp. 8635–8660.
[18] Y. Romano, M. Elad, and P. Milanfar, "The little engine that could: Regularization by denoising (RED)," *SIAM J. Imag. Sci.*, vol. 10, no. 4, pp. 1804–1844, Jan. 2017.
[19] Y. Gandelsman, A. Shocher, and M. Irani, "Double-DIP: Unsupervised image decomposition via coupled deep-image-priors," in *Proc. IEEE/CVF Conf. Comput. Vis. Pattern Recognit. (CVPR)*, Jun. 2019, pp. 11026–11035.
[20] M. Mirza and S. Osindero, "Conditional generative adversarial nets," 2014, *arXiv:1411.1784*.
[21] F. Hashimoto, H. Ohba, K. Ote, A. Teramoto, and H. Tsukada, "Dynamic PET image denoising using deep convolutional neural networks without prior training datasets," *IEEE Access*, vol. 7, pp. 96594–96603, 2019.
[22] H. Sun, L. Peng, H. Zhang, Y. He, S. Cao, and L. Lu, "Dynamic PET image denoising using deep image prior combined with regularization by denoising," *IEEE Access*, vol. 9, pp. 52378–52392, 2021.
[23] J. M. Huang and M. Z. Shen, "Blind deconvolution restoration of turbulent degraded noise image based on total variation," *Opt. Tech.*, vol. 34, no. 4, pp. 525–527, 2008.
[24] L. X. Zhu, M. R. Jiang, and P. M. Fu, "Combining L-like curve method and regularization model to realize multi-frame sun spot image reconstruction," *J. Image Signal Process.*, vol. 10, no. 1, pp. 19–27, 2021.
[25] H. L. Royden and P. Fitzpatrick, *Real Analysis*. New York, NY, USA: Macmillan, 1988, pp. 123–135.
[26] T. F. Chan and C.-K. Wong, "Total variation blind deconvolution," *IEEE Trans. Image Process.*, vol. 7, no. 3, pp. 370–375, Mar. 1998.
[27] J. Pan, Z. Hu, and Z. Su, "ℓ_0-regularized intensity and gradient prior for deblurring text images and beyond," *IEEE Trans. Pattern Anal. Mach. Intell.*, vol. 39, no. 2, pp. 342–355, Feb. 2017.
[28] J. Pan, D. Sun, H. Pfister, and M.-H. Yang, "Deblurring images via dark channel prior," *IEEE Trans. Pattern Anal. Mach. Intell.*, vol. 40, no. 10, pp. 2315–2328, Oct. 2018.
[29] D. P. Kingma and J. Ba, "Adam: A method for stochastic optimization," in *Proc. IEEE Conf. Int. Conf. L. Rep. (ICLR)*, San Diego, CA, USA, Dec. 2015, pp. 1520–1535.
[30] R. Racine, "The telescope point spread function," *Astronomical Soc.*, vol. 108, no. 6, pp. 699–726, 1996.
[31] J. A. Armstrong and L. Fletcher, "A machine-learning approach to correcting atmospheric seeing in solar flare observations," *Monthly Notices Roy. Astronomical Soc.*, vol. 501, no. 2, pp. 2647–2658, Jan. 2021.
[32] T.-Y. Lin, P. Dollar, R. Girshick, K. He, B. Hariharan, and S. Belongie, "Feature pyramid networks for object detection," in *Proc. IEEE Conf. Comput. Vis. Pattern Recognit. (CVPR)*, Jul. 2017, pp. 2117–2125.
[33] C. Ma, Y. Rao, Y. Cheng, C. Chen, J. Lu, and J. Zhou, "Structure-preserving super resolution with gradient guidance," in *Proc. IEEE/CVF Conf. Comput. Vis. Pattern Recognit. (CVPR)*, Jun. 2020, pp. 7769–7778.
[34] O. Kupyn, T. Martyniuk, and J. Wu, "DeblurGAN-V2: Deblurring (orders-of-magnitude) faster and better," in *Proc. IEEE Conf. Comput. Vis. Pattern Recognit. (CVPR)*, Jun. 2019, pp. 8878–8887.
[35] X. Wang, K. Yu, and S. Wu, "ESRGAN: Enhanced super-resolution generative adversarial networks," in *Proc. IEEE Conf. Eur. Conf. Comput. Vis. (ECCV)*, Jun. 2019, pp. 8878–8887.
[36] P. Isola, J.-Y. Zhu, T. Zhou, and A. A. Efros, "Image-to-image translation with conditional adversarial networks," in *Proc. IEEE Conf. Comput. Vis. Pattern Recognit. (CVPR)*, Jul. 2017, pp. 1125–1134.
[37] J.-Y. Zhu, T. Park, P. Isola, and A. A. Efros, "Unpaired image-to-image translation using cycle-consistent adversarial networks," in *Proc. IEEE Int. Conf. Comput. Vis. (ICCV)*, Oct. 2017, pp. 8635–8660.
[38] A. Shocher, N. Cohen, and M. Irani, "Zero-shot super-resolution using deep internal learning," in *Proc. IEEE/CVF Conf. Comput. Vis. Pattern Recognit.*, Jun. 2018, pp. 2223–2232.

YAHUI JIN is currently pursuing the master's degree with the School of Information Science and Engineering, Yunnan University. His current research interest includes image reconstruction.

MURONG JIANG received the Ph.D. degree from the Academy of Engineering Physics of China, in 1997. She is currently a Professor with the School of Information Science and Engineering, Yunnan University. Her current research interests include mathematical method of image processing and intelligent calculation.

LEI YANG received the master's degree from the Yunnan Observatories, Chinese Academy of Sciences, in 2007. He is currently a Senior Engineer with Yunnan Observatories, Chinese Academy of Sciences. His current research interest includes astronomical image reconstruction.

SIZHONG ZOU is currently pursuing the master's degree with the Yunnan Observatories, Chinese Academy of Sciences. His current research interest includes image reconstruction.

LINHAO DENG is currently pursuing the master's degree with the School of Information Science and Engineering, Yunnan University. His current research interest includes image reconstruction.

JUNYI CHEN received the master's degree from the Yunnan Observatories, Chinese Academy of Sciences, in 2006. He is currently a Senior Engineer with Yunnan Observatories, Chinese Academy of Sciences. His current research interest includes high performance computing.